




Letter

Centrality-dependent modification of hadron and jet production in electron-nucleus collisions

Hai Tao Li^a, Ze Long Liu^b, Ivan Vitev^c, *

^a School of Physics, Shandong University, Jinan, Shandong 250100, China

^b Theoretical Physics Department, CERN, 1211 Geneva 23, Switzerland

^c Theoretical Division, Los Alamos National Laboratory, Los Alamos, NM, 87545, USA



ARTICLE INFO

Editor: A. Ringwald

ABSTRACT

Centrality-dependent measurements of hadron and jet cross section attenuation in deep inelastic scattering on nuclei can shed new light on the physics of final-state interactions in nuclear matter, including the path-length dependence of the in-medium parton shower formation and evolution. Recent simulation studies have demonstrated the feasibility of experimental centrality determination in eA reactions at the electron-ion collider via neutron detection in the zero-degree calorimeter. Motivated by these results, we present the first theoretical calculation of the production rate modification for hadrons and jets in central and peripheral ePb collisions. We find that the variation in the suppression of inclusive jet cross section as a function of centrality is less than a factor of two. In more differential measurements, such as the distribution of hadrons versus the hadronization fraction z_h , the difference can be enhanced up to an order of magnitude.

1. Introduction

Reactions with nuclei have been an integral part of the study of quantum chromodynamics (QCD) for more than 40 years [1]. Cold nuclear matter (CNM) effects in particular have been investigated in electron-nucleus (eA) [2,3] and proton-nucleus (pA) collisions [4,5]. These studies include the modification of nuclear structure encoded in parton distribution functions (nPDFs) [6–8], the non-linear physics of high-gluon densities [9–12], and elastic, inelastic and coherent parton scattering in large nuclei [13–16].

Medium-induced radiative corrections have attracted a lot of attention as a natural mechanism of cross section modification in cold nuclear matter. Specifically, they have been applied to interpret [17–22] Drell-Yan and J/ψ suppression at large Feynman- x in minimum bias pA [23,24], and jet modification in central pA at very high energies [25,26]. Furthermore, in the framework of different theoretical formalisms, including parton energy loss, in-medium evolution, a hybrid approach and renormalization group analysis [27–30], bremsstrahlung from final-state interactions was shown to lead to hadron cross section attenuation in semi-inclusive deep inelastic scattering (SIDIS) on nuclei. The overwhelming majority of these calculations have focused on HERMES collaboration measurements on helium (He), neon (Ne),

krypton (Kr) and xenon (Xe) [31–33], but early EMC collaboration results [34,35] show the same type of nuclear modification using carbon (C), copper (Cu) and tin (Sn) as targets.

Final-state radiative corrections are not the only possible explanation of HERMES and EMC results. Models on early hadron formation and absorption in nuclear matter have been developed [36,37] and the possibility of universal fragmentation function modification has also been suggested [38,39]. It was found that light hadron measurements at HERMES do not have sufficient discriminating power to uniquely validate or exclude theoretical models [40,41].

The electron-ion collider (EIC) will provide flexible center-of-mass energies and the opportunity to access final states that have not been studied thus far in SIDIS on nuclei. Recently, significant progress has been made in extending the theory of light and heavy hadron suppression [29,30], and jet and jet substructure modification [42–44] in eA at the EIC. All of these studies have been limited to minimum bias collisions. Centrality-dependent measurements can provide new insights into the physics of final-state interactions in nuclear matter and centrality class determination has been shown to be feasible via neutron tagging [45,46]. To this end, we present theoretical results on hadron and jet modification in central and peripheral electron-lead (ePb) collisions at the future facility.

* Corresponding author.

E-mail addresses: haitao.li@sdu.edu.cn (H.T. Li), zelong.liu@cern.ch (Z.L. Liu), vitev@lanl.gov (I. Vitev).

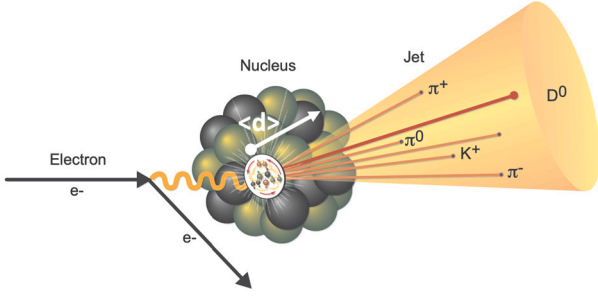


Fig. 1. Illustration of the concept of centrality in electron-nucleus collisions. The struck quark and the jet initiated by it will see nuclear matter of different mean interaction length $\langle d \rangle$.

The rest of this paper is organized as follows: in Sec. 2 we briefly review the theoretical formalism for hadron and jet production on protons and nuclei. Discussion of centrality determination in SIDIS and phenomenological results in central and peripheral ePb collisions are contained in Sec. 3. We present our conclusions in Sec. 4.

2. Theoretical formalism

Recent developments in perturbative QCD have allowed us to place the calculation of semi-inclusive hadron and jet production on the same footing. Using the formalism of jet functions [47,48], the collinear differential hadron and jet cross sections can be written in a similar factorized form

$$\begin{aligned} \frac{d\sigma^{\ell N \rightarrow hX}}{dy_h d^2\mathbf{p}_{T,h}} &= \frac{1}{S} \sum_{i,f} \int_0^1 \frac{dx}{x} \int_0^1 \frac{dz}{z^2} f^{i/N}(x, \mu) \\ &\times \left[\hat{\sigma}^{i \rightarrow f} + f_{\text{ren}}^{\gamma/\ell} \left(\frac{-t}{s+u}, \mu \right) \hat{\sigma}^{\gamma i \rightarrow f} \right] \\ &\times D^{h/f}(z, \mu), \end{aligned} \quad (1)$$

$$\begin{aligned} \frac{d\sigma^{\ell N \rightarrow JX}}{dy_J d^2\mathbf{p}_{T,J}} &= \frac{1}{S} \sum_{i,f} \int_0^1 \frac{dx}{x} \int_0^1 \frac{dz}{z^2} f^{i/N}(x, \mu) \\ &\times \left[\hat{\sigma}^{i \rightarrow f} + f_{\text{ren}}^{\gamma/\ell} \left(\frac{-t}{s+u}, \mu \right) \hat{\sigma}^{\gamma i \rightarrow f} \right] \\ &\times J_f(z, p_T R, \mu). \end{aligned} \quad (2)$$

Here, $f^{i/N}$ is the parton distribution function (PDF) of parton i carrying a fraction x of the nucleon N momentum. We use $\hat{\sigma}^{i \rightarrow f}$ to denote the lepton-parton scattering cross section producing a final-state parton f . The processes that we study as a function of p_T receive contributions from electron scattering at small angles, where the lepton becomes a source of quasi-real photons. The corresponding $\gamma q \rightarrow q(g)$, $\gamma q \rightarrow g(q)$ and $\gamma g \rightarrow q(\bar{q})$ processes contribute to the cross section at order $\alpha_{\text{em}}^2 \alpha_s$ and the Weizsäcker-Williams (WW) distribution of quasi-real photons is given by a perturbative distribution function $f_{\text{ren}}^{\gamma/\ell}(y, \mu)$ [49,50] with s , t , u the lepton-parton Mandelstam variables. The analytical results for $\hat{\sigma}^{i \rightarrow f}$, $\hat{\sigma}^{\gamma i \rightarrow f}$ and $f_{\text{ren}}^{\gamma/\ell}(y, \mu)$ up to $\mathcal{O}(\alpha_{\text{em}}^2 \alpha_s)$ are taken from Ref. [51]. $D^{h/f}$ is the standard fragmentation function (FF) from parton f to hadron h , taking a momentum fraction z . J_f is the semi-inclusive jet function (SiJF) initiated by parton f . When the jet radius R is small, logarithms of the type $\ln R$ can be resummed by evolving the jet function from the jet scale $p_T R$ to the factorization scale μ .

In eA reactions initial-state effects parametrized via nPDFs can alter hadron and jet cross sections. Our main focus in this paper is the centrality dependence of final-state medium-induced radiative corrections and we consider observables that minimize or eliminate the cross section modification due to nPDFs. Parton branching in nuclear matter is described by in-medium splitting kernels $dN_{ji}^{\text{med}}/dzd^2\mathbf{k}_\perp$ for the $i \rightarrow j+k$ channel. We use the results derived in the framework of soft-collinear

effective theory with Glauber gluon interaction (SCET_G) [52,53] and verified using a lightcone wavefunction formalism [54,55].

We calculate numerically the real part of the branching processes,

$$P_{ji}^{\text{med,real}}(z, \mathbf{k}_\perp) = 2\pi \mathbf{k}_\perp^2 \frac{dN_{ji}^{\text{med}}}{dzd^2\mathbf{k}_\perp}, \quad (3)$$

for averaged interaction length $\langle d \rangle$ corresponding to different centrality classes, as illustrated in Fig. 1. The corresponding virtual corrections $P_{ji}^{\text{med,vir}}$ are obtained using flavor and momentum sum rules [56, 57]. Final-state in-medium radiation leads to additional scaling violations [58] in the fragmentation functions and we implement them in medium-modified DGLAP evolution equations [22,28,29,59]

$$\begin{aligned} \frac{dD^{h/i}(x, \mu)}{d \ln \mu^2} &= \sum_j \int_x^1 \frac{dz}{z} [P_{ji}(z, \mu) \\ &+ P_{ji}^{\text{med}}(z, \mu)] D^{h/j} \left(\frac{x}{z}, \mu \right). \end{aligned} \quad (4)$$

We solve these equations numerically using HOPPET [60].

The SiJFs used to calculate the semi-inclusive jet cross sections also receive medium-induced radiative corrections. We implement them at next-to-leading order as shown in Refs. [42,43,61,62]. The results for quark and gluon initiated jets of transverse momentum p_T and radius parameter R read

$$\begin{aligned} J_q^{\text{med}}(z, p_T R, \mu) &= \left[\int_{z(1-z)p_T R}^\mu d^2\mathbf{k}_\perp f_{q \rightarrow qg}^{\text{med}}(z, \mathbf{k}_\perp) \right]_+ \\ &+ \int_{z(1-z)p_T R}^\mu d^2\mathbf{k}_\perp f_{q \rightarrow gq}^{\text{med}}(z, \mathbf{k}_\perp), \end{aligned} \quad (5)$$

$$\begin{aligned} J_g^{\text{med}}(z, p_T R, \mu) &= \left[\int_{z(1-z)p_T R}^\mu d^2\mathbf{k}_\perp \left(h_{gg}(z, \mathbf{k}_\perp) \left(\frac{z}{1-z} + z(1-z) \right) \right) \right]_+ \\ &+ n_f \left[\int_{z(1-z)p_T R}^\mu d^2\mathbf{k}_\perp f_{g \rightarrow q\bar{q}}(z, \mathbf{k}_\perp) \right]_+ \\ &+ \int_{z(1-z)p_T R}^\mu d^2\mathbf{k}_\perp \left(h_{gg}(x, \mathbf{k}_\perp) \left(\frac{1-z}{z} + \frac{z(1-z)}{2} \right) \right) \\ &+ n_f f_{g \rightarrow q\bar{q}}(z, \mathbf{k}_\perp), \end{aligned} \quad (6)$$

where we have denoted $dN_{ji}^{\text{med}}/dzd^2\mathbf{k}_\perp \equiv f_{i \rightarrow jk}^{\text{med}}(z, \mathbf{k}_\perp)$ for brevity. In Eq. (6)

$$h_{gg}(z, \mathbf{k}_\perp) = \frac{f_{g \rightarrow gg}^{\text{med}}(z, \mathbf{k}_\perp)}{\frac{z}{1-z} + \frac{1-z}{z} + z(1-z)}. \quad (7)$$

In the equations above all, singularities when $z \rightarrow 1$ are regularized by the plus-distribution function that has the standard definition.

3. Centrality dependent nuclear modification

To study the centrality dependent nuclear modification, we are motivated by recent simulations of constraints on nuclear geometry in eA reactions using the Monte Carlo event generator BeAGLE [46]. The idea behind this more differential approach is to measure the energy deposited in the zero-degree calorimeter [45] at the EIC and correlate it to collision centrality, and the effective path length $\langle d \rangle$. A subset of

Table 1

Selected centrality classes in e Pb collisions at the EIC, the corresponding effective length of cold nuclear matter seen by the scattered parton, and the ratio relative to the one in minimum bias (0 – 100 %) collisions.

Centrality	0 – 1%	0 – 3%	0 – 10%	60 – 100%	80 – 100%	90 – 100%	0 – 100%
$\langle d \rangle [fm]$	9.09	8.48	7.61	2.88	2.71	2.71	4.40
$\langle d \rangle / \langle d \rangle_{\text{min.bias}}$	2.07	1.93	1.73	0.65	0.62	0.62	1.00

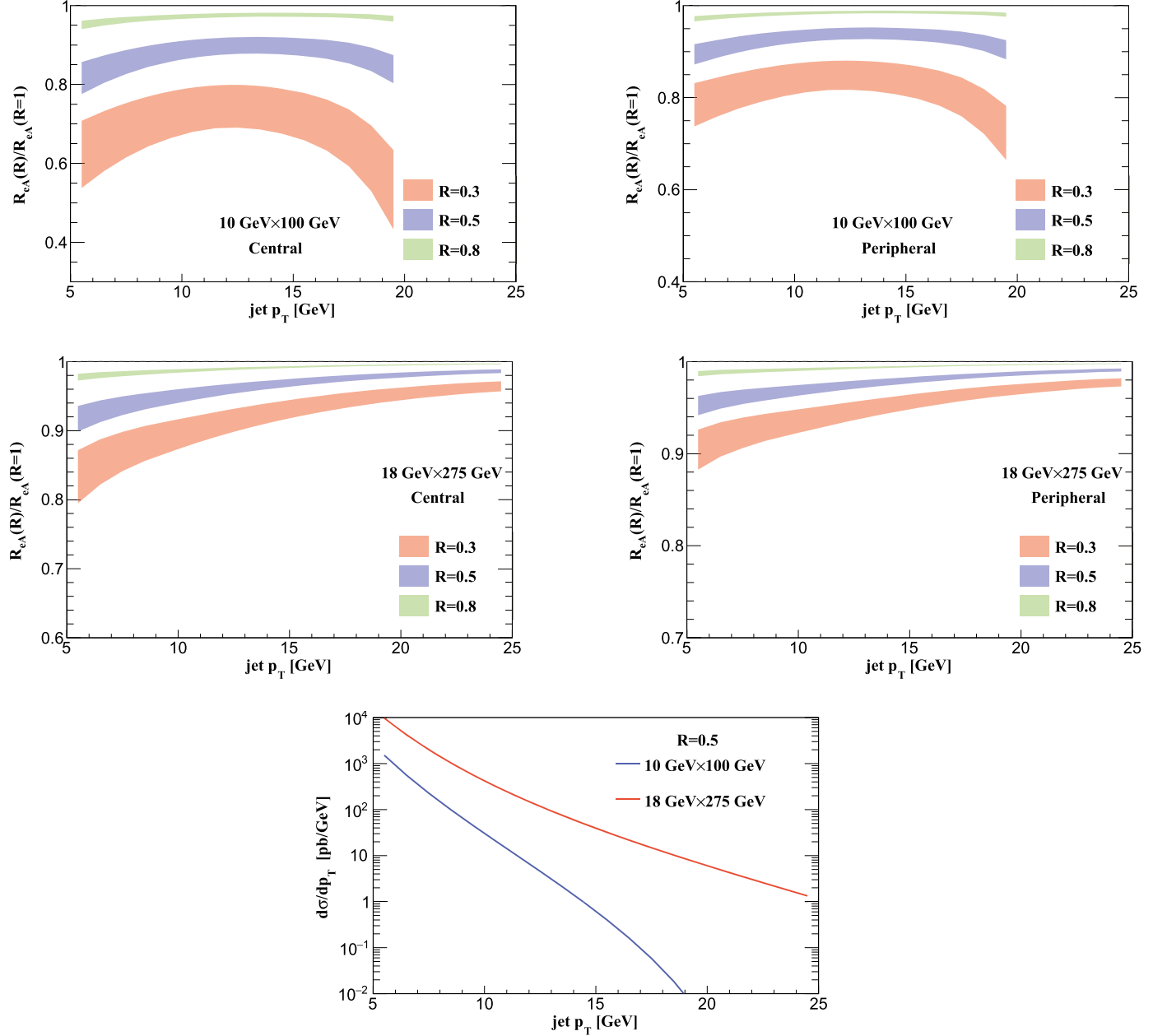


Fig. 2. Relative modifications of the inclusive jet cross section $R_{eA}(R)/R_{eA}(R=1)$ for three radius choices $R=0.3, 0.5, 0.8$ in the rapidity interval $2 < \eta < 4$. The upper panels are for $10 \text{ GeV} \times 100 \text{ GeV}$ e Pb collisions and the middle panels are for $18 \text{ GeV} \times 275 \text{ GeV}$ e Pb collisions. Central reactions are on the left and peripheral reactions are on the right. The baseline ep cross sections for $R=0.5$ at the two different energies are also shown in the bottom panel.

effects, such as shadowing or assumed initial particle formation time, were studied and found to not significantly affect the energy distribution in the ZDC. The correlation between the centrality classes and the energy deposition remains robust when such effects are taken into account in simulation.

With this in mind, the average interaction length of a parton in a Pb nucleus as a function of centrality obtained in BeAGLE is given in

Table 1. In the top 0-1% central events $\langle d \rangle$ is twice as large as the one in minimum bias collisions. In the most peripheral 90-100% events $\langle d \rangle$ is almost twice as small as the minimum bias one. In this paper, we pick two representative examples of centrality selection - a central - 0-10% class and a peripheral 80-100% class. Next, we calculate grids of in-medium splitting functions [52–55] while constraining nuclear geometry to yield the enhancement or reduction of the average

interaction length relative to the minimum bias one as given in Table 1. We average over the position of hard scattering vertex along the line of parton propagation, but keep the splitting kernel differential in $(z, |\mathbf{k}_\perp|)$ as needed for the in-medium jet function evaluation and in-medium DGLAP evolution. While the grids are obtained numerically, recent analytic advances [30] have allowed us to identify the leading medium size and kinematic dependencies of the branching

$$f_{i \rightarrow jk}^{\text{med}}(z, \mathbf{k}_\perp) \sim \frac{\langle k_\perp^2 \rangle L^2}{\lambda_{q,g} E} \dots \quad (8)$$

This implies that nuclear effects will increase from peripheral to central collisions, will decrease as the parton energy E grows in the nuclear rest frame, and will depend on the medium transport properties $\langle k_\perp^2 \rangle / \lambda_{q,g}$.

With the numerically evaluated splitting functions at hand and the theoretical framework described in Sec. 2 we now turn to phenomenology. In our calculations for the baseline ep collisions we use CT14nlo PDF sets [63] with the strong coupling constant provided by LHAPDF6 [64]. For the case of semi-inclusive hadron production, fragmentation functions into light pions are taken directly from the HKNS parameterization in Ref. [65]. Heavy quark fragmentation into D - and B -mesons at the scale $\mu = 2m_Q$ is evaluated perturbatively using heavy quark effective theory (HQET) [66,67] and evolved to a higher scale. When we consider reactions with nuclei, such as the $e\text{Pb}$ case of interest, we use the nCTEQ15FullNuc PDF sets [6]. In comparison to Ref. [29], where we varied the transport parameters up and down by a factor of two relative to the nominal fit value to HERMES data, here we focus on the $v > 10$ GeV region and reduce their range to $0.096 \text{ GeV}^2/\text{fm} < \langle k_\perp^2 \rangle / \lambda_q < 0.168 \text{ GeV}^2/\text{fm}$, $0.043 \text{ GeV}^2/\text{fm} < \langle k_\perp^2 \rangle / \lambda_q < 0.075 \text{ GeV}^2/\text{fm}$.

We first consider jets reconstructed with a radius parameter R and define the centrality dependent nuclear modification in electron-nucleus collisions through the ratio

$$R_{eA}(R) = \frac{1}{\Delta_b T_A(b)} \frac{\int_{\eta_1}^{\eta_2} d\sigma/d\eta dp_T|_{eA}}{\int_{\eta_1}^{\eta_2} d\sigma/d\eta dp_T|_{ep}}. \quad (9)$$

Here, the nuclear thickness function at impact parameter b is

$$T_A(b) = \int_{-\infty}^{\infty} \rho(z, b) dz, \quad (10)$$

and $\Delta_b = 2\pi b db$ is the differential area around the impact parameter b such that $\sum_b \Delta_b T_A(b) = A$. In other words, $R_{eA}(R)$ is the per nucleon cross section modification for the relevant impact parameters corresponding to the centrality class. Earlier work on hadron and jet production in minimum bias eA collisions has already provided useful guidance on how to study final-state interactions [29,42,43]. In particular, they can be separated from initial-state nuclear PDFs [6,7] by taking the ratio of nuclear modification for a small radius jet to the modification for a large radius jet $R_{eA}(R)/R_{eA}(R=1)$. This strategy works very well, eliminating initial-state effects to less than a few % [42,43].

In Fig. 2 we show the double modification ratio $R_{eA}(R)/R_{eA}(R=1)$ for three different choices $R = 0.3$ (red band), 0.5 (blue band), and 0.8 (green band). The bands correspond to cold nuclear matter transport parameters in the ranges quoted above. The idea behind normalizing this observable to the R_{eA} for a large radius jet is that final-state effect for $R = 1$ will be minimal. Even though the medium induced parton shower is broader than the vacuum one, most of it will be contained in a unit radius. Conversely, by choosing smaller radii an increasingly larger fraction of the shower energy will be redistributed outside of the jet cone, leading to cross section suppression. We also choose the forward proton/nucleus going direction $2 < \eta < 4$ since the jet energy in this kinematic region is the smallest in the rest frame of the nucleus, leading to larger final-state effects. The top row of panels shows $10 \text{ GeV} (e) \times 100 \text{ GeV}$ (Pb) collision and the bottom row of panels is for 18 GeV

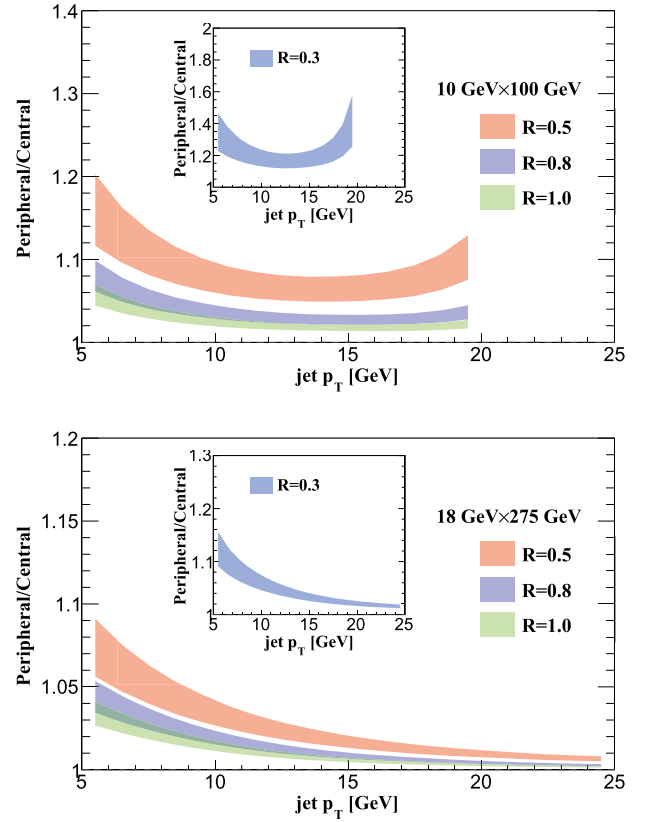


Fig. 3. Ratio of per-nucleon jet cross sections in peripheral and central collisions for the jet rapidity interval is $2 < \eta < 4$ and $R = 0.3$ (inset), 0.5 (red), 0.8 (blue), and 1.0 (green). The upper panel is for $10 \text{ GeV} \times 100 \text{ GeV}$ $e\text{Pb}$ collisions and the bottom one is for $18 \text{ GeV} \times 275 \text{ GeV}$ $e\text{Pb}$ collisions.

$(e) \times 275 \text{ GeV}$ (Pb) collisions. On the left we show the 0-10% centrality selection and the 80-100% centrality class is on the right.

Our calculations show that the nuclear modification is the largest at relatively small transverse momenta. At the same time, it depends on the steepness of the p_T spectra (shown in the bottom panel of Fig. 2 for ep collisions) and the effects become larger again close to the kinematic edges of phase space, as seen in the upper panels of Fig. 2. For large radius jets the relative modification $R_{eA}(R=0.8)/R_{eA}(R=1)$ is small, $\leq 5\%$. On the other hand, for small radius jets $R_{eA}(R=0.3)/R_{eA}(R=1)$ in central $e\text{Pb}$ reactions can show up to 40% suppression. At higher center of mass energies the modification is smaller, as expected, and decreases monotonically with p_T . By comparing the left and right panels of Fig. 2 we see clearly that final-state effects depend on the thickness of nuclear matter.

Another method to directly investigate the interaction length dependence of final-state cold nuclear matter effects using jet production is to compare the cross sections in peripheral and central collisions. Thus, we define the ratio as

$$\frac{\text{Peripheral}}{\text{Central}}(J) = \frac{\frac{1}{\Delta_b T_A(b)} \int_{\eta_1}^{\eta_2} \frac{d\sigma}{d\eta dp_T} |_{eA, \text{Peri.}}}{\frac{1}{\Delta_b T_A(b)} \int_{\eta_1}^{\eta_2} \frac{d\sigma}{d\eta dp_T} |_{eA, \text{Cent.}}}, \quad (11)$$

where the initial-state effects are reduced and most of the contribution is from final-state interactions. In fact, the nPDF parametrization we use [6] does not include centrality dependence. In principle, nuclear effects on structure functions can depend on the path length seen by the struck parton [14]. Separation between such effects and global nuclear structure modification will be important to better understand the residual dependence in Eq. (13). As discussed above, the medium induced energy loss is smaller and the per-nucleon cross section is larger for peripheral collisions. Thus, the ratio defined in Eq. (13) is expected

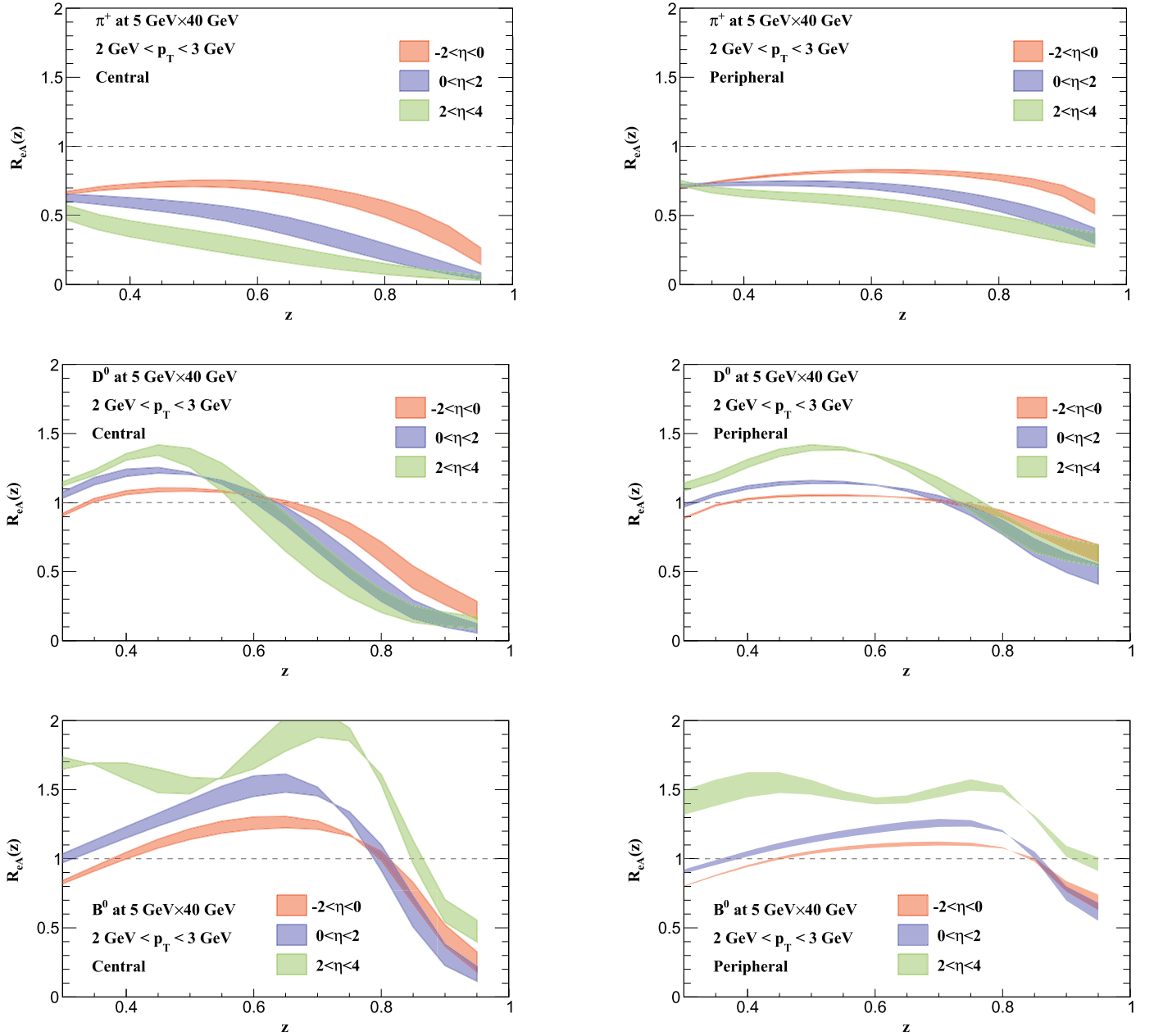


Fig. 4. In-medium corrections to π^+ (top panels), D^0 (middle panels) and B^0 (bottom panels) production as a function of z at the EIC in 5 GeV(e) \times 40 GeV(A) collision. Red bands, blue bands, and green bands correspond to $-2 < \eta < 0$, $0 < \eta < 2$ and $2 < \eta < 4$, respectively. Results for central collisions (0 – 10% centrality) are shown on the left, and results for peripheral collisions (80 – 100% centrality) are shown on the right.

to be larger than one. Fig. 3 displays our predictions for 10 GeV (e) \times 100 GeV (Pb) and 18 GeV (e) \times 275 GeV (Pb) collisions in the forward rapidity region for various jet radii. The $R = 0.3$ case is shown in the insets since, as expected, the ratio is much larger than in other cases and is very sensitive to the thickness of the nuclear matter in kinematic regions where the jet p_T distribution is steeper in particular when the collision energy is small. For 10 GeV (e) \times 100 GeV (Pb) collisions the ratio can be around 1.1 for $R = 0.5$ and $R = 0.8$ in the small jet p_T region. It shows only about a few percent deviation from one for $R = 1$. The ratio in the large p_T region is enhanced since jets are produced close to the edges of phase space. For 18 GeV (e) \times 275 GeV (Pb) collisions, the ratio decreases with increasing jet p_T and is smaller than 1.1 for all of the cases. The R dependence indicates that the energy loss for larger radii is smaller which is consistent with Fig. 2. In summary, the centrality class-dependent modification in matter is clearly observed in Fig. 3.

Next, we discuss the cross-section modification for hadron production at the EIC, including π^+ and the heavy D_0 and B_0 mesons. As shown in [29], the following double ratio as a function of momentum fraction z is a suitable observable for cold nuclear matter tomography at the EIC

$$R_{eA}^h(z) = \frac{N^h(p_T, \eta, z) \big|_{eA}}{N^{\text{inc}}(p_T, \eta) \big|_{eA}} \cdot \frac{N^h(p_T, \eta, z) \big|_{ep}}{N^{\text{inc}}(p_T, \eta) \big|_{ep}}. \quad (12)$$

Here, we use the shorthand notation $N^h(p_T, \eta, z) \equiv d\sigma^h/d\eta dp_T dz$ for the distribution of hadrons versus the hadronization fraction z and $N^{\text{inc}}(p_T, \eta) \equiv d\sigma^J/d\eta dp_T$ for the distribution of large radius jets. In practice we integrate over suitably chosen rapidity and transverse momentum bins before taking the ratio. The idea behind normalizing by $N^{\text{inc}}(p_T, \eta)$ is to once again minimize initial-state effects and emphasize

physics of final-state interactions in nuclear matter. For eA collisions we can further define per-nucleon cross sections by dividing out the $1/\Delta_b T_A(b)$ geometric factor.

Our results for $R_{ePb}^h(z)$ are shown in Fig. 5. We consider electron-proton/nucleus collisions with energy 5 GeV (e) \times 40 GeV (A), and the transverse momenta of final-state hadrons are fixed in the range 2 GeV to 3 GeV. Consequently, the momentum fraction z distribution corresponds to the variation of ν constrained by the kinematics of the scattered electron in experiment. The left column of panels is for the 0 – 10% central events, and the right column is for 80 – 100% peripheral events. For each hadron species, the red, blue and green bands correspond to the predictions in rapidity regions $-2 < \eta < 0$, $0 < \eta < 2$ and $2 < \eta < 4$, respectively. Just as in the case of jet production, the bands reflect the variation of the nuclear matter transport parameter constrained by high ν HERMES data. Top to bottom rows show the differential π^+ , D^0 and B^0 modification. Because lower energy partons receive larger medium corrections induced by the final-state interactions in the nucleus, the medium modification is more significant in the forward rapidity region $2 < \eta < 4$. In this region the energy of the final-state parton is lower in the nuclear rest frame in comparison, for example, to backward rapidity. It is instructive to observe that for light hadrons at large z the differential cross section suppression can reach a factor of two even in peripheral collisions. In central events the energy loss effect can lead to more than an order of magnitude reduction. For heavy flavor, just as in minimum bias reactions [29], $R_{ePb}^h(z)$ shows transition from suppression at large z to enhancement at small z because of the non-monotonic behavior of the heavy quark fragmentation function into heavy mesons [66,67]. In central reactions nuclear effects are noticeably larger.

To compare the cross section modification in central and peripheral collisions for differential hadron distributions quantitatively, we define

$$\frac{\text{Peripheral}}{\text{Central}}(h) = \frac{R_{eA}^h(z)|_{eA,\text{Peri.}}}{R_{eA}^h(z)|_{eA,\text{Cent.}}} \quad (13)$$

and note that the baseline ep cross sections will drop out. As we expect, central collisions result in more significant medium corrections than peripheral ones, as shown in Fig. 4. The steep fragmentation distribution when $z \rightarrow 1$ enhances the differences for light pions to an order of magnitude. As we go forward in rapidity the enhancement in $\text{Peripheral/Central}(h)$ extends to smaller z . For D^0 mesons this enhancement can also be very significant when $z \rightarrow 1$ but at intermediate fragmentation fractions the double ratio can dip below unity – a consequence of the transition from suppression to enhancement in $R_{eA}^h(z)$. The qualitative behavior is similar for B^0 mesons.

4. Conclusions

We presented theoretical predictions for the nuclear modification of semi-inclusive hadron and jet production in ePb collisions at the EIC as a function of centrality. We took advantage of recent simulations that were able to demonstrate robust correlation between centrality classes in eA and energy deposition in the zero-degree calorimeter, and to determine the mean interaction length seen by partons. We constructed observables that minimize initial-state nPDF effects and are sensitive to the inelastic final-state interactions of the struck parton in the nucleus. Future measurements of these observables at the EIC can provide essential information on the path length dependence of parton shower formation and hadronization in cold nuclear matter.

Our theoretical results indicate that the dependence of in-medium shower formation and energy loss on the transport properties and size of the nuclear medium can be easily identified and studied at the EIC. The exact sensitivity, however, depends on the choice of observables. We found that for inclusive jets of small radius at moderate center-of-mass energies and at forward rapidities the per-nucleon cross sections variation between 0-10% and 80-100% collision can reach a factor of

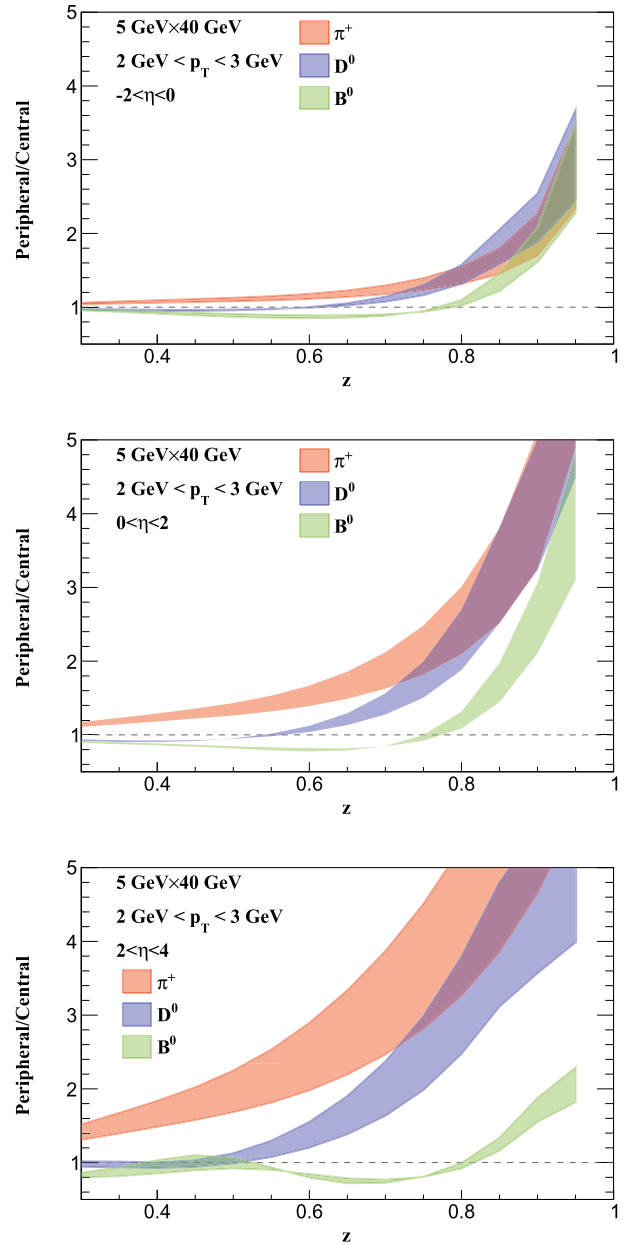


Fig. 5. The ratio of R_{eA}^h in peripheral to central collisions. The electron and proton/nucleus beam energies, p_T and η ranges are the same as in Fig. 4. We show π^+ (red), D^0 (blue) and B^0 (green). From top to bottom panels cover backward to forward rapidities.

40%. Because of the high integrated luminosity that EIC is expected to deliver [3], such peripheral-to-central differences will be easily measurable, but they are smaller than the differences in the mean interaction length $\langle d \rangle$ seen by the jet. The reason for this is that even for $R = 0.3$ only a fraction of the medium-induced shower is redistributed outside of the jet cone.

Hadron measurements at forward rapidity can be performed at even lower center-of-mass energies. Our theoretical calculations showed that the per-nucleon differential particle distributions versus the fragmentation fraction z_h depend much more significantly on centrality. For light pions at large z_h the peripheral-to-central ratio can reach a factor of 5, exceeding the ratio of effective interaction lengths for these centrality classes. Furthermore, the nuclear modification due to final-state interactions and its centrality variation are strong enough to be detected near mid rapidity and even at backward rapidity. The nuclear cross sec-

tion modification also depends on the hadron flavor and has a predicted non-monotonic behavior for D - and B -mesons. We conclude by pointing out that in the future it will be important to explore the centrality dependence of other more differential jet observables such as jet substructure.

Declaration of competing interest

The authors declare that they have no known competing financial interests or personal relationships that could have appeared to influence the work reported in this paper.

Data availability

Data will be made available on request.

Acknowledgements

The authors wish to thank R. Dupre for suggesting the calculation of centrality-dependent hadron and jet quenching at the EIC and P. Zurita for bringing early EMC measurements to our attention. We further acknowledge helpful discussion with W. Chang and M. Baker on centrality determination in DIS and thank W. Chang for providing us with the effective interaction lengths $\langle d \rangle$ in eA obtained with BeAGLE. This research is performed in the framework of the HEFTY topical collaboration for nuclear theory. I. Vitev is supported by the LDRD program at LANL and by the U.S. Department of Energy under Contract No. 89233218CNA000001. H.T. Li is supported by the National Science Foundation of China under grant No. 12275156. Z.L. Liu is funded by the European Union (ERC, grant agreement No. 101044599, JANUS). Views and opinions expressed are however those of the authors only and do not necessarily reflect those of the European Union or the European Research Council Executive Agency. Neither the European Union nor the granting authority can be held responsible for them.

References

- [1] J. Aubert, G. Bassompierre, K. Becks, C. Best, E. Böhm, X. de Bouard, F. Brasse, C. Broll, S. Brown, J. Carr, et al., *Phys. Lett. B* 123 (1983) 275.
- [2] Proceedings, Probing Nucleons and Nuclei in High Energy Collisions: Dedicated to the Physics of the Electron Ion Collider: Seattle (WA), United States, October 1 - November 16, 2018, WSP, 2020, arXiv:2002.12333.
- [3] R. Abdul Khalek, et al., *Nucl. Phys. A* 1026 (2022) 122447, arXiv:2103.05419.
- [4] J.L. Albacete, et al., *Int. J. Mod. Phys. E* 22 (2013) 1330007, arXiv:1301.3395.
- [5] J.L. Albacete, et al., *Nucl. Phys. A* 972 (2018) 18, arXiv:1707.09973.
- [6] K. Kovarik, et al., *Phys. Rev. D* 93 (2016) 085037, arXiv:1509.00792.
- [7] K.J. Eskola, P. Paakkinen, H. Paukkunen, C.A. Salgado, *Eur. Phys. J. C* 77 (2017) 163, arXiv:1612.05741.
- [8] R. Abdul Khalek, J.J. Ethier, J. Rojo, NPDF, *Eur. Phys. J. C* 79 (2019) 471, arXiv:1904.00018.
- [9] I.I. Balitsky, L.N. Lipatov, *Sov. J. Nucl. Phys.* 28 (1978) 822, *Yad. Fiz.* 28 (1978) 1597.
- [10] L.D. McLerran, R. Venugopalan, *Phys. Rev. D* 49 (1994) 3352, arXiv:hep-ph/9311205.
- [11] J. Jalilian-Marian, A. Kovner, A. Leonidov, H. Weigert, *Phys. Rev. D* 59 (1998) 014014, arXiv:hep-ph/9706377.
- [12] Y.V. Kovchegov, *Phys. Rev. D* 60 (1999) 034008, arXiv:hep-ph/9901281.
- [13] E. Wang, X.-N. Wang, *Phys. Rev. Lett.* 89 (2002) 162301, arXiv:hep-ph/0202105.
- [14] J.-W. Qiu, I. Vitev, *Phys. Lett. B* 587 (2004) 52, arXiv:hep-ph/0401062.
- [15] I. Vitev, *Phys. Rev. C* 75 (2007) 064906, arXiv:hep-ph/0703002.
- [16] M. Arratia, Y. Song, F. Ringer, B.V. Jacak, *Phys. Rev. C* 101 (2020) 065204, arXiv:1912.05931.
- [17] S. Gavin, J. Milana, *Phys. Rev. Lett.* 68 (1992) 1834.
- [18] F. Arleo, *Phys. Lett. B* 532 (2002) 231, arXiv:hep-ph/0201066.
- [19] R.B. Neufeld, I. Vitev, B.-W. Zhang, *Phys. Lett. B* 704 (2011) 590, arXiv:1010.3708.
- [20] H. Xing, Y. Guo, E. Wang, X.-N. Wang, *Nucl. Phys. A* 879 (2012) 77, arXiv:1110.1903.
- [21] F. Arleo, C.-J. Naim, S. Platchkov, *J. High Energy Phys.* 01 (2019) 129, arXiv:1810.05120.
- [22] Z.-B. Kang, I. Vitev, H. Xing, *Phys. Rev. C* 92 (2015) 054911, arXiv:1507.05987.
- [23] M.B. Johnson, et al., FNAL E772, *Phys. Rev. Lett.* 86 (2001) 4483, arXiv:hep-ex/0010051.
- [24] M.J. Leitch, W.M. Lee, M.E. Beddo, C.N. Brown, T.A. Carey, T.H. Chang, W.E. Cooper, C.A. Gagliardi, G.T. Garvey, D.F. Geesaman, et al., FNAL E866/NuSea Collaboration, *Phys. Rev. Lett.* 84 (2000) 3256.
- [25] G. Aad, et al., ATLAS, *Phys. Lett. B* 748 (2015) 392, arXiv:1412.4092.
- [26] A. Adare, et al., PHENIX, *Phys. Rev. Lett.* 116 (2016) 122301, arXiv:1509.04657.
- [27] F. Arleo, *Eur. Phys. J. C* 30 (2003) 213, arXiv:hep-ph/0306235.
- [28] N.-B. Chang, W.-T. Deng, X.-N. Wang, *Phys. Rev. C* 89 (2014) 034911, arXiv:1401.5109.
- [29] H.T. Li, Z.L. Liu, I. Vitev, arXiv:2007.10994, 2020.
- [30] W. Ke, I. Vitev, arXiv:2301.11940, 2023.
- [31] A. Airapetian, et al., HERMES, *Eur. Phys. J. C* 20 (2001) 479, arXiv:hep-ex/0012049.
- [32] A. Airapetian, et al., HERMES, *Phys. Lett. B* 577 (2003) 37, arXiv:hep-ex/0307023.
- [33] A. Airapetian, et al., HERMES, *Nucl. Phys. B* 780 (2007) 1, arXiv:0704.3270.
- [34] J. Ashman, B. Badelek, G. Baum, J. Beaufays, C.P. Bee, C. Benchouk, I.G. Bird, S.C. Brown, M.C. Caputo, H.W.K. Cheung, et al., *Z. Phys. C, Part. Fields* 52 (1991) 1.
- [35] A. Arvidson, J. Aubert, G. Bassompierre, K. Becks, C. Benchouk, C. Best, E. Böhm, X. de Bouard, F. Brasse, C. Broll, et al., *Nucl. Phys. B* 246 (1984) 381, ISSN 0550-3213.
- [36] A. Accardi, V. Muccifora, H.-J. Pirner, *Nucl. Phys. A* 720 (2003) 131, arXiv:nucl-th/0211011.
- [37] B. Kopeliovich, J. Nemchik, E. Predazzi, A. Hayashigaki, *Nucl. Phys. A* 740 (2004) 211, arXiv:hep-ph/0311220.
- [38] R. Sassot, M. Stratmann, P. Zurita, *Phys. Rev. D* 81 (2010) 054001, arXiv:0912.1311.
- [39] P. Zurita, arXiv:2101.01088, 2021.
- [40] A. Accardi, F. Arleo, W. Brooks, D. D'Enterria, V. Muccifora, *Riv. Nuovo Cimento* 32 (2010) 439, arXiv:0907.3534.
- [41] R. Dupré, Ph.D. thesis, Lyon, IPN, 2011.
- [42] H.T. Li, I. Vitev, *Phys. Rev. Lett.* 126 (2021) 252001, arXiv:2010.05912.
- [43] H.T. Li, Z.L. Liu, I. Vitev, *Phys. Lett. B* 827 (2022) 137007, arXiv:2108.07809.
- [44] K. Devereaux, W. Fan, W. Ke, K. Lee, I. Moul, arXiv:2303.08143, 2023.
- [45] L. Zheng, E.C. Aschenauer, J.H. Lee, *Eur. Phys. J. A* 50 (2014) 189, arXiv:1407.8055.
- [46] W. Chang, E.-C. Aschenauer, M.D. Baker, A. Jentsch, J.-H. Lee, Z. Tu, Z. Yin, L. Zheng, arXiv:2204.11998, 2022.
- [47] Z.-B. Kang, F. Ringer, I. Vitev, *J. High Energy Phys.* 10 (2016) 125, arXiv:1606.06732.
- [48] L. Dai, C. Kim, A.K. Leibovich, *Phys. Rev. D* 94 (2016) 114023, arXiv:1606.07411.
- [49] C. von Weizsacker, *Z. Phys.* 88 (1934) 612.
- [50] E. Williams, *Phys. Rev.* 45 (1934) 729.
- [51] P. Hinderer, M. Schlegel, W. Vogelsang, *Phys. Rev. D* 92 (2015) 014001, Erratum: *Phys. Rev. D* 93 (2016) 119903, arXiv:1505.06415.
- [52] G. Ovanesyan, I. Vitev, *J. High Energy Phys.* 06 (2011) 080, arXiv:1103.1074.
- [53] Z.-B. Kang, F. Ringer, I. Vitev, *J. High Energy Phys.* 03 (2017) 146, arXiv:1610.02043.
- [54] M.D. Sievert, I. Vitev, *Phys. Rev. D* 98 (2018) 094010, arXiv:1807.03799.
- [55] M.D. Sievert, I. Vitev, B. Yoon, *Phys. Lett. B* 795 (2019) 502, arXiv:1903.06170.
- [56] J.C. Collins, J.-w. Qiu, *Phys. Rev. D* 39 (1989) 1398.
- [57] Y.-T. Chien, A. Emerman, Z.-B. Kang, G. Ovanesyan, I. Vitev, *Phys. Rev. D* 93 (2016) 074030, arXiv:1509.02936.
- [58] G. Altarelli, G. Parisi, *Nucl. Phys. B* 126 (1977) 298.
- [59] W. Ke, I. Vitev, arXiv:2204.00634, 2022.
- [60] G.P. Salam, J. Rojo, *Comput. Phys. Commun.* 180 (2009) 120, arXiv:0804.3755.
- [61] Z.-B. Kang, F. Ringer, I. Vitev, *Phys. Lett. B* 769 (2017) 242, arXiv:1701.05839.
- [62] H.T. Li, I. Vitev, *J. High Energy Phys.* 07 (2019) 148, arXiv:1811.07905.
- [63] S. Dulat, T.-J. Hou, J. Gao, M. Guzzi, J. Huston, P. Nadolsky, J. Pumplin, C. Schmidt, D. Stump, C.P. Yuan, *Phys. Rev. D* 93 (2016) 033006, arXiv:1506.07443.
- [64] A. Buckley, J. Ferrando, S. Lloyd, K. Nordstrom, B. Page, M. Ruffenacht, M. Schoenher, G. Watt, *Eur. Phys. J. C* 75 (2015) 132, arXiv:1412.7420.
- [65] M. Hirai, S. Kumano, T.-H. Nagai, K. Sudoh, *Phys. Rev. D* 75 (2007) 094009, arXiv:hep-ph/0702250.
- [66] E. Braaten, K.-m. Cheung, S. Fleming, T.C. Yuan, *Phys. Rev. D* 51 (1995) 4819, arXiv:hep-ph/9409316.
- [67] K.-m. Cheung, T.C. Yuan, *Phys. Rev. D* 53 (1996) 1232, arXiv:hep-ph/9502250.